DOI 10.24425/aee.2025.153910

Model-free control of a DC–DC boost converter based on the averaging of inductor current

ANGEL MAUREIRA [1]✉, SEBASTIÁN RIFFO [1], CARLOS RESTREPO [1,2], CATALINA GONZÁLEZ-CASTAÑO [3,4], MARCO RIVERA [5,6]

[1] *Laboratory of Applications in Smart Grids, Faculty of Engineering, Universidad de Talca*
Curicó 3340000, Chile

[2] *Principal investigator MIGA 7820436*
Chile

[3] *Energy Transformation Center, Faculty of Engineering, Universidad Andres Bello*
Santiago 7500971, Chile

[4] *Assistant Investigator MIGA 7820436*
Chile

[5] *Power Electronics, Machines and Control (PEMC) Research Institute*
Department of Electrical and Electronic Engineering, Faculty of Engineering, University of Nottingham
15 Triumph Rd, Lenton, Nottingham NG7 2GT, UK

[6] *Energy Conversion and Power Electronics Laboratory (LCEEP)*
Vicerrectoría Académica, Universidad de Talca
Talca 3460000, Chile

e-mail: ✉ *amaureira15@alumnos.utalca.cl, {sebastian.riffo/crestrepo}@utalca.cl, catalina.gonzalez@unab.cl, marco.rivera@nottingham.ac.uk*

(Received: 30.09.2024, revised: 16.05.2025)

Abstract: This work aims to present a model-free predictive control (MF–PC) technique that is robust to parameter and model changes to control a boost converter. The MF–PC proposed is based on calculating and updating the value of the current slope in the inductor at each sampling instant and using it to predict the future value of the current to define the optimal state to apply in the next step. To evaluate the performance of this proposal, a fair comparison is made between MF–PC and classical finite control set model predictive control (FCS–MPC) under reference changes and physical converter parameter variations in a boost converter. The experimental results show that the proposed method is robust against parameters and model changes compared to FCS–MPC. Additionally, the proposed controller reduces the number of sensed variables compared to the conventional FCS–MPC and has the simplicity required for converters operating at high frequencies.

Key words: boost converter, digital control, power electronics, predictive control

1. Introduction

In recent decades, model predictive control (MPC) has received significant attention within the academic field, generating a variety of research articles dedicated to its review, applications, and theoretical results [1–5], this is due to its favorable characteristic of working with non-linear systems, generally restricted, with multiple inputs and outputs in a clear and unified manner [6]. Particularly, in the field of power electronics, as an alternative to classic linear control strategies, various proposals for digital controllers derived from predictive control have emerged, generally applied to converters and electrical drives [7, 8]. Thus, taking advantage of the benefits it has over this type of system, such as its intuitive and easy-to-understand concepts, its ability to work with multiple switches and objective variables to control, the constraints and nonlinearities that can be easily included, and the resulting controller which is generally easy to implement [6].

Model-free predictive control (MF-PC) theory has emerged as an alternative to conventional MPC to address problems arising from poor model estimation or the loss of model accuracy, mainly caused by variations in the system's environmental conditions or operating point [9–11]. Besides the fact that it is not possible to know with certainty the model of the system to be controlled, either due to its high mathematical complexity or because, on some occasions, it has yet to be known a priori what will be connected to the system [9]. In any case, the MPC control will degrade, which will cause sub-optimal operation.

Although MPC is widely used in power electronics, most of the applications reported in the literature have been focused on ac-dc and dc-ac converters [12–14]. This is also the case with MF–PC applications, with few works focused on dc-dc applications. However, the increase in the implementation of microgeneration systems, supported by the growth of dc-based renewable energies, such as photovoltaic systems and other dc-powered loads, promotes dc-based energy distribution on a residential scale, this being supported by several studies that highlight the potential of dc microgrids and their involved dc-dc converters, minimizing energy losses during its distribution [15–17]. Therefore, more efficient dc-dc converters with lower costs, higher reliability, and reduced output current ripple are expected to drive the increased deployment of residential dc microgrids.

Additionally, dc-dc power converters have an important role in various energy applications, such as aircraft, electric vehicles, ships, dc homes, data center and microgrids [18]. This evidence shows the need to evaluate and study novel approaches to the elements involved in this type of converter, as is the case of promising control strategies such as MF–PC.

Considering those mentioned above, this paper proposes MF–PC on the dc-dc boost converter, shown in Fig. 1, to estimate the inductor's positive and negative current slopes with high accuracy and low computational cost. Based on the comprehensive review of state-of-the-art regarding control design for dc-dc converter applications based on MF–PC, this research makes the following contributions:

1. A new control with simple implementation and low computational cost is proposed, capable of operating at high frequency, required in dc-dc converter applications.
2. The proposed control is a model-free strategy independent of the converter modeling or parameters, depending only on the inductor current slopes.
3. Compared to conventional MPC, the proposed strategy reduces the number of variables sensed on the converter necessary for its control.
4. A fair comparison between MF–PC and MPC strategies for a boost converter, considering reference changes and variations in physical converter parameters.

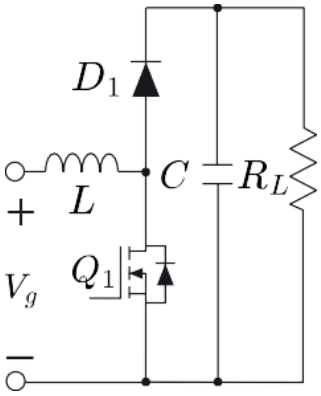

Fig. 1. Boost converter diagram

The rest of the paper is organized as follows: Section 2 shows the control description used to estimate the inductor current slopes of the dc-dc boost converter. Next, Section 3 presents the experimental results of the implementation of the proposed controller and a comparison with the finite control set model predictive control (FCS–MPC). Finally, the conclusions and future work are presented in Section 4.

2. MF–PC based on the inductor current averaging operating principle

2.1. Slopes calculation based on inductor current measurement

The operating principle of the proposed control is based on the dynamics of the inductor current in switched converters, assuming that its value will always be positive or, in other words, that it will work in continuous current mode. The inductor current in classical second-order dc-dc power converters has a triangular waveform due to the semiconductors' switching. Depending on the switching state, the slope of this current will be positive or negative. If the switching state is 1, meaning the switch Q_1 is closed, the slope will always be positive, and vice versa. An example of both switching states of Q_1 is presented in Fig. 2.

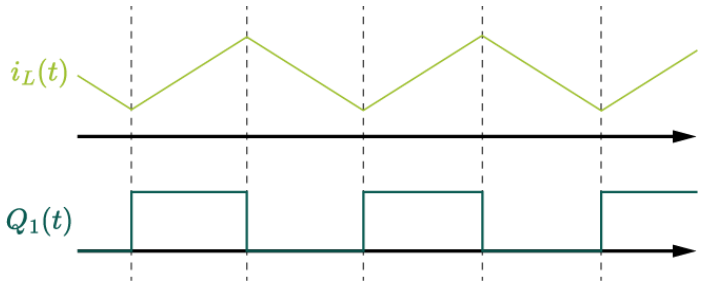

Fig. 2. Generic current waveform of a switching converter

Considering the above, it is possible to define a model-free control law that depends only on the value of the positive and negative slopes of the inductor current, which will be calculated and updated at each sampling instant k. To obtain an approximation of the next value of the current, a regressive approximation of the derivative is employed as follows:

$$\frac{\mathrm{d}}{\mathrm{dt}} i_L \cong \frac{\Delta i_L}{\Delta T} = \frac{i_L(k) - i_L(k-1)}{T_s}, \tag{1}$$

where: $i_L(k)$ is the value of the current at the k instant and T_s the sampling time. Using (1), these two slopes can be calculated as follows in a discrete system with the proposed control topology:

$$m_k^1 = \begin{cases} 10000, & \text{if} \quad k = 0 \\ m_{k-1}^1, & \text{if} \quad Q_1 = 0 \quad \text{or} \quad \dfrac{i_L(k) - i_L(k-1)}{T_s} \leq 0 \\ \dfrac{i_L(k) - i_L(k-1)}{T_s}, & \text{if} \quad Q_1 = 1 \quad \text{or} \quad \dfrac{i_L(k) - i_L(k-1)}{T_s} > 0 \end{cases}, \tag{2}$$

$$m_k^2 = \begin{cases} -10000, & \text{if} \quad k = 0 \\ m_{k-1}^2, & \text{if} \quad Q_1 = 1 \quad \text{or} \quad \dfrac{i_L(k) - i_L(k-1)}{T_s} \geq 0 \\ \dfrac{i_L(k) - i_L(k-1)}{T_s}, & \text{if} \quad Q_1 = 0 \quad \text{or} \quad \dfrac{i_L(k) - i_L(k-1)}{T_s} < 0 \end{cases}, \tag{3}$$

whereas (2) is the positive slope calculation when the switching state is 1, and (3) is the negative slope calculation when the switching state is 0, thus defining the values of m_k^1 and m_k^2, respectively. For the controller startup ($k = 0$), a high and arbitrary slope value is assumed, being $m_0^1 = 10\,000$ in the case of the positive slope, and $m_0^2 = -10\,000$ in the negative slope. Thus, the controller will be able to correctly execute the control law when starting, knowing the relationship between the switching state and the increasing or decreasing behavior of the current.

Figure 3 shows a generic waveform of the inductor in steady-state and how, for each step, there is a slope m^1 and m^2 directly proportional to the difference between the current value of the inductor current i_L and its value in the previous step and inversely proportional to T_s.

It is also possible to calculate the average of the slopes to reduce the prediction error in systems with more noise. Through (4), a simple moving average can be obtained for the case of a positive

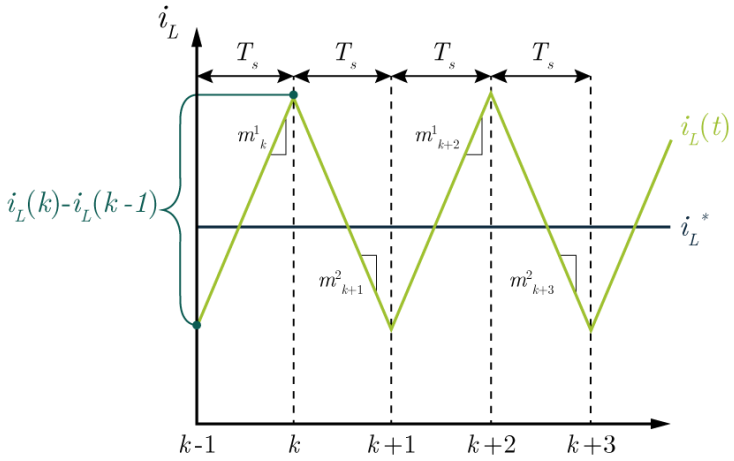

Fig. 3. Inductor current waveform under MF–PC based on inductor current averaging

slope, using an unweighted average of the previous N data points.

$$m^1_{\mathrm{SMA}}(k,N) = \frac{1}{N}\sum_{j=k-N+1}^{k} i_L(j). \tag{4}$$

2.2. Current prediction and calculation of optimal switching state

Once the value of the slopes $\boldsymbol{m^1}$ and $\boldsymbol{m^2}$ has been calculated and updated, it is possible to estimate the future value of the inductor current for both switching states based on the current value of $\boldsymbol{i_L}$ and the sampling time $\boldsymbol{T_s}$, as follows:

$$\boldsymbol{i_L}(\boldsymbol{k}+\boldsymbol{1}) = \begin{cases} \boldsymbol{i_L}(\boldsymbol{k}) + \boldsymbol{m^1_k}\cdot\boldsymbol{T_s}, & \text{if} \quad \boldsymbol{Q_1}=\boldsymbol{1} \\ \boldsymbol{i_L}(\boldsymbol{k}) + \boldsymbol{m^2_k}\cdot\boldsymbol{T_s}, & \text{if} \quad \boldsymbol{Q_1}=\boldsymbol{0} \end{cases}. \tag{5}$$

With these predictions, and the inductor current reference $i_L^*(k+1)$ for the next step, the cost function is computed to define the optimal switching state. For this work the cost functions for each slope are defined as:

$$\mathrm{CF_{up}} = i_L^*(k+1) - i_{L_{\mathrm{up}}}(k+1), \tag{6}$$

$$\mathrm{CF_{down}} = i_L^*(k+1) - i_{L_{\mathrm{down}}}(k+1). \tag{7}$$

Finally, the state of the switching signal is set by comparing the cost functions, where $S=1$ when $\mathrm{CF_{down}} > \mathrm{CF_{up}}$, and $S=0$ when $\mathrm{CF_{up}} > \mathrm{CF_{down}}$. The flowchart in Fig. 4 summarizes the proposed methodology.

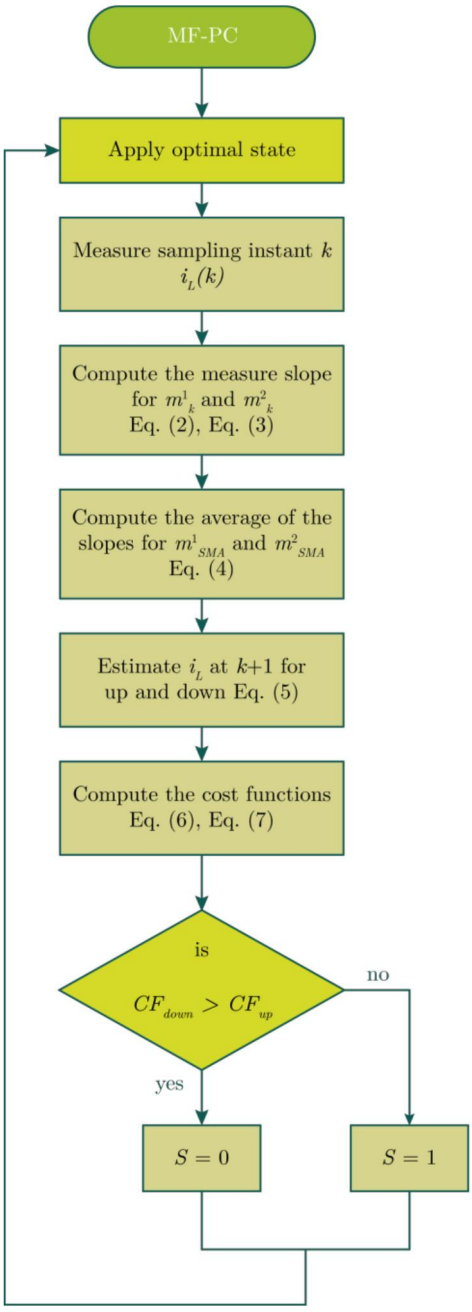

Fig. 4. Flowchart of the proposed MF–PC

2.3. Description of FCS–MPC

Due to the discrete nature of power converters and their finite number of switching states, the implementation of the MPC controller can be reduced to predict the future behavior of the system by calculating each of its possible states and evaluating which of them is the most appropriate control action and applying it directly on the converter switch. Thus, defining the problem of determining a control action based on the state of the switches $\boldsymbol{S(k)}$, which allows one to bring the state variables $\boldsymbol{x(t)}$ closer to the desired reference value $\boldsymbol{x^*(t)}$ [1]

A simplified generic diagram of the FCS–MPC implementation on a power converter connected to a load is presented in Fig. 5.

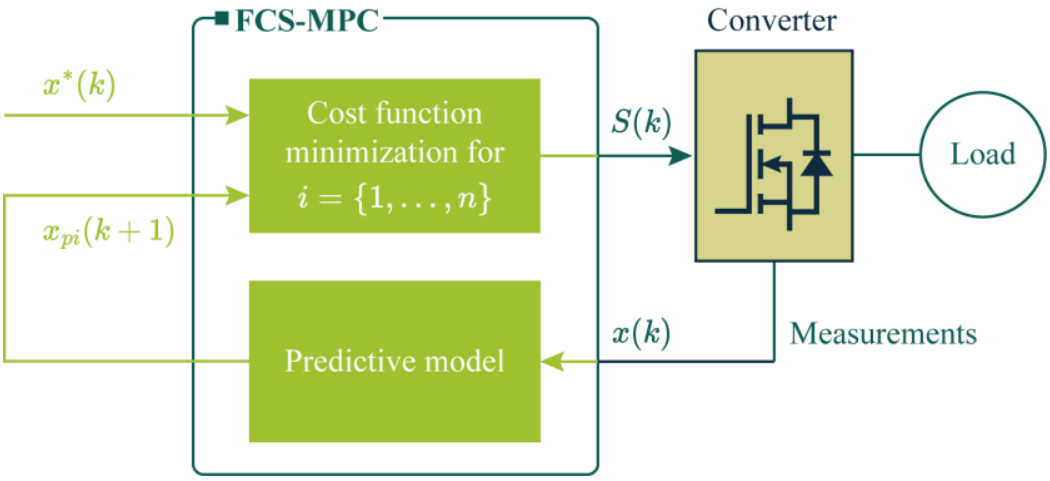

Fig. 5. Generic control diagram of FCS–MPC

For each of the finite control actions S_i, with $i = \{1, \ldots, n\}$, together with the measurements of the current value of $\boldsymbol{x}(k)$, it is possible to predict the future value of the states based on the function f_p of the form $\boldsymbol{x_{pi}}(k+1) = f_p\{\boldsymbol{x}(k), S_i\}$, where the equations necessary for the prediction are derived from the discrete model of the converter and the system parameters, this being the main difference with the proposed MF–PC method. The cost function f_g, which will determine the control action, depends on the predictions made $\boldsymbol{x_{pi}}(k+1)$ and the desired value of the reference $\boldsymbol{x}^*$, being: $g_i = f_g\left\{\boldsymbol{x}^*(k+1), \boldsymbol{x_{pi}}(k+1)\right\}$. From the previous expression, it follows that for the evaluation of g, the value of the future reference $\boldsymbol{x}^*(k+1)$ is necessary. However, because T_s is small enough compared to the dynamics of the system, it can be assumed equal to the current value $\boldsymbol{x}^*(k)$.

An expression commonly used to define f_g is the absolute error between the prediction and the reference: $g_i = \left|\boldsymbol{x}^*(k+1) - \boldsymbol{x_{pi}}(k+1)\right|$, which is calculated with each prediction value and adopts the control action that gives the lowest value of g_i. Figure 6 exemplifies the generic algorithm used in FCS–MPC.

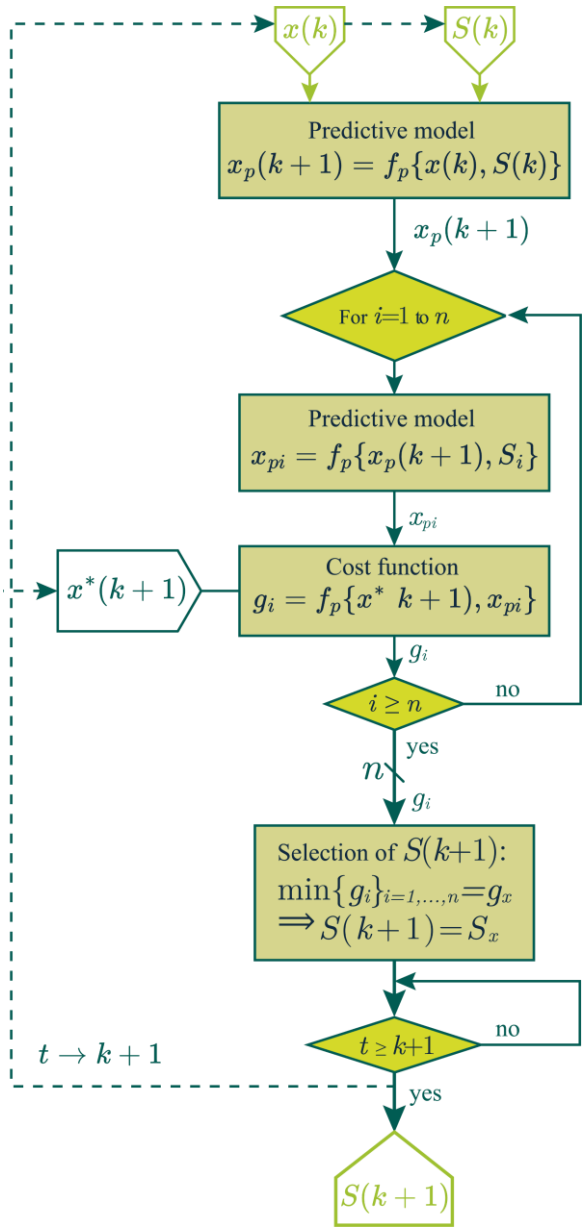

Fig. 6. Generic FCS–MPC algorithm

2.4. Model of boost converter to implement FCS–MPC

The model used for the FCS–MPC implementation is based on a bilinear representation of the boost converter, which can be expressed as follows:

$$\boldsymbol{x}(\boldsymbol{k}+\mathbf{1}) = \boldsymbol{A}\boldsymbol{x}(\boldsymbol{k}) + \boldsymbol{u}(\boldsymbol{k})\,\boldsymbol{\beta}(\boldsymbol{x}(\boldsymbol{k})) + \boldsymbol{d}, \tag{8}$$

where the state variables are given by the vector $\boldsymbol{x} \in R^{\mathbf{2}}$, with $\boldsymbol{x} = (\boldsymbol{i_L}\mathbf{v_0})$, and the current state of the input $\boldsymbol{u}(\boldsymbol{k})$. This model presents a linear part composed of the matrix $\boldsymbol{A} \in R^{\mathbf{2\times 2}}$, and another non-linear produced by the product between $\boldsymbol{u}(\boldsymbol{k})\, y\boldsymbol{\beta}(\boldsymbol{x}(\boldsymbol{k})) : R^{\mathbf{2}} \rightarrow R$, defining this as:

$$\boldsymbol{\beta}(\boldsymbol{x}(\boldsymbol{k})) = \boldsymbol{B}\boldsymbol{x}(\boldsymbol{k}) + \boldsymbol{b}, \tag{9}$$

with $\boldsymbol{B} \in R^{\mathbf{2\times 2}}$, $\boldsymbol{b} \in R^{\mathbf{2}}$, and $\boldsymbol{d} \in R^{\mathbf{2}}$. The matrix parameters $\boldsymbol{A}$, $\boldsymbol{B}$, $\boldsymbol{b}$ and $\boldsymbol{d}$ are:

$$\boldsymbol{A} = \begin{bmatrix} \mathbf{1} & -\dfrac{\boldsymbol{T_s}}{\boldsymbol{L}} \\ \dfrac{\boldsymbol{T_s}}{\boldsymbol{C}} & \mathbf{1} - \dfrac{\boldsymbol{T_s}}{\boldsymbol{R_L C}} \end{bmatrix}, \tag{10}$$

$$\boldsymbol{B} = \begin{bmatrix} \mathbf{0} & \dfrac{\boldsymbol{T_s}}{\boldsymbol{L}} \\ -\dfrac{\boldsymbol{T_s}}{\boldsymbol{C}} & \mathbf{0} \end{bmatrix}, \tag{11}$$

$$\boldsymbol{b} = \begin{bmatrix} \mathbf{0} \\ \mathbf{0} \end{bmatrix}, \tag{12}$$

$$\boldsymbol{d} = \begin{bmatrix} \dfrac{\boldsymbol{T_s V_g}}{\boldsymbol{L}} \\ \mathbf{0} \end{bmatrix}. \tag{13}$$

3. Experimental results

This section presents the results of implementing the proposed MF–PC technique to regulate the inductor current in a boost converter supplying a resistive load. Furthermore, to evaluate the robustness of the controller, its performance is analyzed under parametric variations in the passive elements of the physical converter.

3.1. Controller implementation

A Rapid Control Prototyping (RCP) configuration is used for the implementation through a real-time simulation platform, which acts as the controller, and a physical boost converter. The platform is a Plexim RT Box 2 that operates with a $\boldsymbol{T_s}$ of 5 µs, and interfaces with the converter using its analog and digital inputs and outputs. Those that will be responsible for the current measurement of the inductor current $\boldsymbol{i_L}(\boldsymbol{t})$, the load voltage $\boldsymbol{V_0}(\boldsymbol{t})$ to implement FCS–MPC, and

the digital output with the control signal that will be applied to the switch $\boldsymbol{Q_1}$ of the boost converter. This sampling time value is used for both MF–PC and FCS–MPC, since both methods involve a variable switching frequency. Therefore, there is no fixed value of the switching frequency, although a maximum limit of 100 kHz can be defined in cases where there is a duty cycle of 50 percent by considering $\boldsymbol{T_s}$ of 5 µs. The implementation diagram of this control system is shown in Fig. 7.

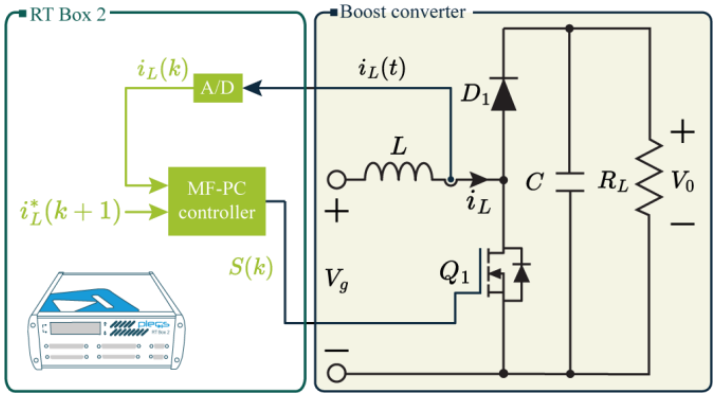

Fig. 7. Block diagram for the proposed MF–PC based on the inductor current averaging

The parameters of the boost converter are presented in Table 1, where the values and characteristics of its passive and semiconductor elements are specified. The converter and the equipment used for its implementation are illustrated in Fig. 8, highlighting all devices involved in the control and experimental measurements. It is important to note that the converter design is based on a switching frequency of 100 kHz, a current ripple of approximately 0.7 A, and a supply voltage of 12 V.

Table 1. Selected components for the boost converter

Parameter	**Component**
Capacitor C	TDK, rated for 100 V, 100 kHz *C5750X7S2A106M230KB* $25 \times 10\,\mu$F
Inductor L	Wurth Elektronik, rated for 9 A, 100 kHz, 74435584700, $2 \times 47\,\mu$H
Power semiconductor Q_1	Power MOSFET Infineon, IRFB4110
Diode D_1	Vishay, V60100C

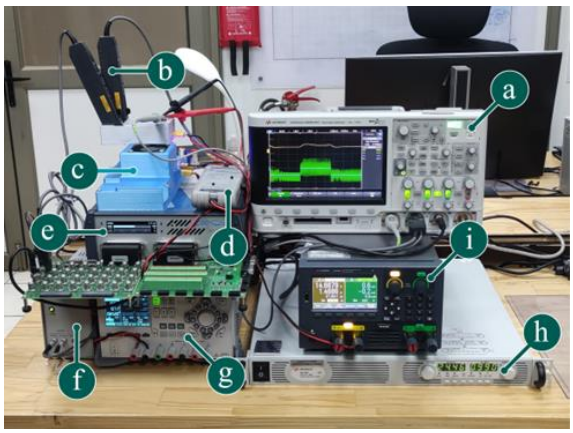

Fig. 8. Experimental setup: (a) oscilloscope, (b) current probes, (c) boost converter, (d) differential voltage probe, (e) RT Box 2 with analog and digital breakout boards, (f) current probe power supply, (g) MOSFET driver power supply, (h) input voltage power supply, and (i) dc electronic load

3.2. Experimental results

The experimental results are presented in Fig. 9, where the proposed controller is compared with the classic FCS–MPC using a spider chart that focuses on the following performance measures: steady-state error (SSE), prediction error (PE), current ripple (R), computational cost (CC) as a percentage (where the FCS–MPC is 100 percent), and the number of sensed variables (NSV). SSE, PE, and R, are measured in amperes and presented as absolute values.

In all cases, the parameters R_L, L, and C are physically modified directly on the power converter, while the nominal values are preserved in the controller's code. The experimental evaluation consists of comparing the behavior of the controllers in the following cases: in nominal conditions (case 1), when the value of the inductor L is reduced to 50 percent (case 2), when the value of the capacitor C is reduced to 50 percent (case 3), and when the load resistance value R_L is reduced to 50 percent (case 4). The results are presented in columns a), b), c) and d) of Fig. 9. All these tests will be accompanied by a variation of the current reference value i_L^* between 2 to 3 amperes for the first three evaluations and between 3 to 4 amperes in the last evaluation to avoid discontinuous current operation. Table 2 summarizes the different cases to be evaluated and the respective values of the converter parameters.

Table 2. Different evaluation cases

Converter	**V_g [Vdc]**	**Parameters**	**Nominal values**	**Case 1 (a)**	**Case 2 (b)**	**Case 3 (c)**	**Case 4 (d)**
Boost	12	R_L [Ω]	10	–	–	–	5
		L [μH]	94	–	47	–	–
		C [μF]	250	–	–	100	–
		Ref [A]	2–3	–	-	–	3–4

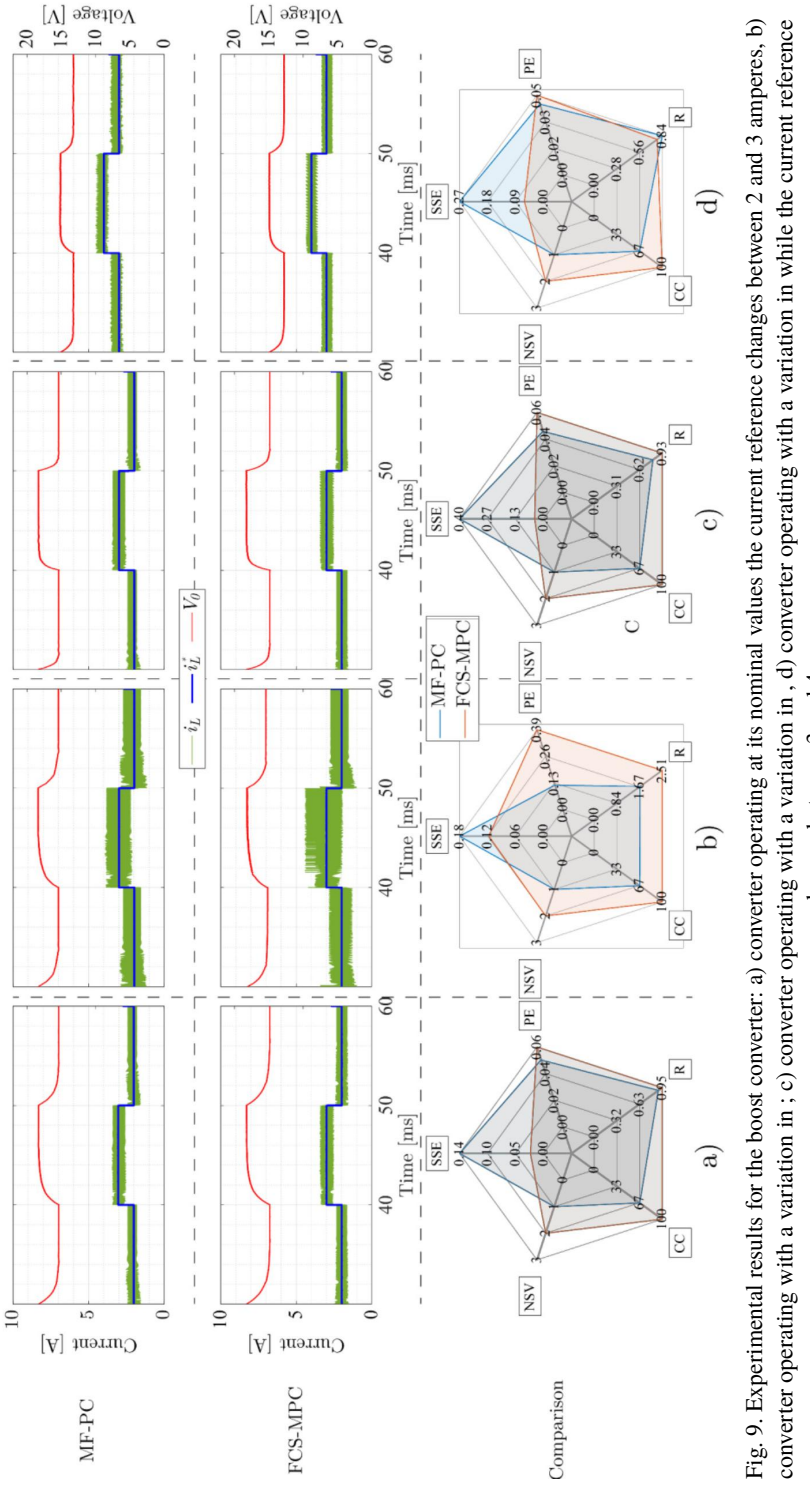

Fig. 9. Experimental results for the boost converter: a) converter operating at its nominal values the current reference changes between 2 and 3 amperes, b) converter operating with a variation in , c) converter operating with a variation in while the current reference changes between 3 and 4 amperes

The results obtained under nominal conditions show how the proposed strategy has a higher performance in terms of PE, R, and CC, but there is a higher SSE than that obtained by the FCS–MPC controller. When faced with variations in the physical parameters of the converter, changes in the inductor are the ones that most affect the dynamics of both controllers; however, the proposed strategy has the best response to these changes and is superior to the compared technique in all indicators.

4. Conclusions

A model-free predictive control approach based on the inductor current averaging for the dc-dc boost converter has been presented. A comparison with the FCS–MPC approach was performed, evaluating the steady-state error, prediction error, current ripple, computational cost, and the number of sensed variables required by each control technique.

In all cases, the proposed MF–PC controller shows a superior dynamic characteristic to the FCS–MPC. Under normal conditions, it presents significant advantages in terms of prediction error, current ripple, and computational cost. In the case of SSE, the MF–PC method generates a higher value when the converter follows the low-value reference, and it is observed that it is proportional to the operating point at which the converter is working. In the case of R, this is directly related to the prediction made by the controller, which is better in most cases for the MF–PC method since it adjusts the slope values at each step by adjusting the prediction, only having a lower performance when making variations in the capacitor value where the FCS–MPC method takes advantage thanks to its additional measurement of the output voltage. A similar, or even higher, dynamic is shown when subjected to variations in the physical parameters of the converter, especially when changing the inductor value, where the FCS–MPC presents lower performance. This is something to highlight, considering that the proposal only requires the measurement of one variable, while the FCS–MPC needs to sense two variables (inductor current and capacitor voltage). Therefore, the proposed controller offers significant advantages compared to the classical predictive method in terms of implementation, since its execution implies a lower CC with a smaller NSV for the control of the converter. Additionally, because of the nature of these types of controllers, the proposed MF–PC presents a lower prediction error in all cases, demonstrating its adaptive capacity and robustness in prediction even when there are changes in the converter parameters.

Future work in development is the extension of the proposed control to other converter topologies such as buck, buck-boost, and non-inverting buck-boost. And improvements in the control strategy are also being studied to implement this controller at high fixed switching frequencies.

Acknowledgements

This work was supported in part by Thematic Network RIBIERSE-CYTED (723RT0150) and in part by the Chilean Government under projects ANID/FONDECYT/3220126, ANID/FONDECYT/1231015, SERC Chile ANID/FONDAP/1522A0006, and the Millenium Institute on Green Ammonia as Energy Vector MIGA (ANID/Millennium Science Initiative Program/ICN2021 023).

References

[1] Kouro S., Cortes P., Vargas R., Ammann U. *et al.*, *Model Predictive Control – a Simple and Powerful Method to Control Power Converters*, IEEE Transactions on Industrial Electronics, vol. 56, no. 6, pp. 1826–1838 (2009), DOI: 10.1109/TIE.2008.2008349.

[2] Rodriguez J., Cortes P., *Predictive control of power converters and electrical drives*, John Wiley & Sons (2012).

[3] Rodriguez J., Kazmierkowski M., Espinoza J. *et al.*, *State of the Art of Finite Control Set Model Predictive Control in Power Electronics*, IEEE transactions on Industrial Informatics, vol. 9, no. 2, pp. 1003–1016 (2013), DOI: 10.1109/TII.2012.2221469.

[4] Vazquez S., Rodriguez J., Rivera M. *et al.*, *Model Predictive Control for Power Converters and Drives: Advances and Trends*, IEEE Transactions on Industrial Electronics, vol. 64, no. 2, pp. 935–947 (2017), DOI: 10.1109/TIE.2016.2625238.

[5] Vazquez S., Leon J., Franquelo L. *et al.*, *Model Predictive Control: A Review of Its Applications in Power Electronics*, IEEE Industrial Electronics Magazine, vol. 8, no. 1, pp. 16–31 (2014), DOI: 10.1109/MIE.2013.2290138.

[6] Orłowska-Kowalska T., Blaabjerg F., Rodriguez J., *Advanced and intelligent control in power electronics and drives*, 531: Springer (2014).

[7] Cortes P., Kazmierkowski M.P., Kennel R.M. *et al.*, *Predictive Control in Power Electronics and Drives*, IEEE Transactions on Industrial Electronics, vol. 55, no. 12, pp. 4312–4324 (2008), DOI: 10.1109/TIE.2008.2007480.

[8] Karamanakos P., Liegmann E., Geyer T. *et al.*, *Model Predictive Control of Power Electronic Systems: Methods, Results, and Challenges*, IEEE Open Journal of Industry Applications, vol. 1, pp. 95–114 (2020), DOI: 10.1109/OJIA.2020.3020184.

[9] Khalilzadeh M., Vaez-Zadeh S., Rodriguez J. *et al.*, *Model-Free Predictive Control of Motor Drives and Power Converters: A Review*, IEEE Access, vol. 9, pp. 105733–105747 (2021), DOI: 10.1109/ACCESS.2021.3098946.

[10] Stenman A., *Model-free predictive control*, Proceedings of the 38th IEEE Conference on Decision and Control, Phoenix, AZ, USA, pp. 3712–3717 (1999), DOI: 10.1109/CDC.1999.827931.

[11] Nauman M., Shireen W., Hussain A., *Model-Free Predictive Control and Its Applications*, Energies, vol. 15, 5131 (2022), DOI: 10.3390/en15145131.

[12] Jlasii I., Marques A., *Open-circuit fault-tolerant operation of permanent magnet synchronous generator drives for wind turbine systems using a computationally efficient model predictive current control*, IET Electric Power Applications, vol. 15, no. 7, pp. 837–846 (2021), DOI: 10.1049/elp2.12062.

[13] Hredzak B., Agelidis V.G., Jang M., *A Model Predictive Control System for a Hybrid Battery-Ultracapacitor Power Source*, IEEE Transactions on Power Electronics, vol. 29, no. 3, pp. 1469–1479 (2014), DOI: 10.1109/TPEL.2013.2262003.

[14] Wei Y., Young H., Wang F. *et al.*, *Generalized Data-Driven Model-Free Predictive Control for Electrical Drive Systems*, IEEE Transactions on Industrial Electronics, vol. 70, no. 8, pp. 7642–7652 (2023), DOI: 10.1109/TIE.2022.3210563.

[15] Kakigano H., Nomura M., Ise T., *Loss evaluation of DC distribution for residential houses compared with AC system*, The 2010 International Power Electronics Conference – ECCE ASIA, Sapporo, Japan, pp. 480–486 (2010), DOI: 10.1109/IPEC.2010.5543501.

[16] Gelani H.E., Dastgeer F., Nasir M. *et al.*, *AC vs. DC Distribution Efficiency: Are We on the Right Path?*, Energies, vol. 14, 4039 (2021), DOI: 10.3390/en14134039.

[17] Gelani H.E., Dastgeer F., Siraj K. *et al*., *Efficiency Comparison of AC and DC Distribution Networks for Modern Residential Localities*, Appl. Sci., vol. 9, no. 582 (2019), DOI: 10.3390/app9030582.

[18] Revathi B.S., Prabhakar M., *Solar PV Fed DC Microgrid: Applications, Converter Selection, Design and Testing*, IEEE Access, vol. 10, pp. 87227–87240 (2022), DOI: 10.1109/ACCESS.2022.3199701.